AIAA JOURNAL
Vol. 38, No. 9, September 2000

Shape Design Sensitivity Analysis and Optimization of Elasto–Plasticity with Frictional Contact

Nam H. Kim,* Kyung K. Choi,† and Jiun S. Chen‡
University of Iowa, Iowa City, Iowa 52242

A shape design sensitivity analysis and optimization are proposed for the infinitesimal elasto–plasticity with a frictional contact condition. Rate-independent plasticity is considered with a return mapping algorithm and a von Mises yield criterion. The contact condition is formulated using the penalty method and the modified coulomb friction law. A continuum-based shape design sensitivity formulation is developed for structural and frictional contact variational equations. The direct differentiation method is used to compute the displacement sensitivity, and the sensitivities of various performance measures are computed from the displacement sensitivity. Path dependency of the sensitivity equation due to the constitutive relation and friction is discussed. It is shown that no iteration is required to solve the sensitivity equation. Response analysis and the proposed sensitivity formulation are implemented using the mesh-free method where the mesh distortion problem can be resolved. Numerical examples show accurate results of the proposed method compared to the finite difference method. Difficulties in the sensitivity formulation for the finite deformation problem are discussed.

I. Introduction

BECAUSE of the recent development of computational mechanics, it is now possible to analyze practical examples of complicated structural problems. Many design engineers, who are not satisfied with response analysis alone, have keen interests in the methodology of the design. For more than two decades, significant research effort has been focused on the rate of response with respect to the changes in structural shape under shape design sensitivity analysis (DSA). Analysis of the design sensitivity information is the most important and costly procedure in the automated optimum design process. It supplies useful quantitative information to the design engineer about the direction of the desired design change. In a classical linear problem, DSA research has proved the differentiability of the solution of the response analysis using the linear operator theory and has derived specific sensitivity expressions for various problems.[1] A result worthy of attention in linear DSA is that the original response and the sensitivity of the response belong to the same kinematically admissible space and have the same regularities.

Owing to the development of the response analysis capability, engineers have directed their interest to the nonlinear problems that are dealt with efficiently. Because many design application problems are accompanied by plastic deformation, the design sensitivity of nonlinear problems has been actively developed, and many research results are reported. In the procedure of nonlinear response analysis, the projection, called a return mapping, of the elastic trial stress is carried out to satisfy the variational inequality (VI) through an iteration in the stress space.[2] The DSA, on the other hand, computes the rate of change of the projected response in the tangential direction of the constraint set without iteration. Note that the sensitivity analysis is linear and can be computed without iteration even though the response analysis is nonlinear.[3] Unlike the nonlinear elastic problem, the sensitivity equation of the plastic problem requires sensitivity of the stress and internal evolution variables at the previous time. The sensitivity equation is solved at each time without iteration, and the sensitivity of the stress and evolution variables are stored for the sensitivity equation at the next time step. For this reason, the sensitivity equation at each load step computes the material derivative of the incremental displacement and the material derivative of the total displacement can be obtained by summing all of the material derivatives of the incremental displacements. The process of the sensitivity computation is divided into two parts. The first is computing the sensitivity of the incremental displacement, and the second is updating the sensitivity of the stress and the evolution variables using the incremental displacement sensitivity.

The Newton–Raphson iteration method is frequently used for response analysis of a nonlinear variational equation using a tangent operator. If the tangent operator is exact, this method guarantees the quadratic convergence when the initial estimate is close enough to the solution.[4] Even if the tangent operator is not exact, the response analysis may be converged by consuming a greater number of iterations. However, in DSA, the inexact tangent operator causes the error in the sensitivity results. In Ref. 3, the accuracy of the sensitivity coefficients using the consistent tangent operator and the rate-form tangent operator are discussed. For the major research results of DSA in plasticity, refer to Refs. 3 and 5–10.

Because most of the plastic deformations of materials occur through contact with another structure, contact analysis is inevitable in practical applications. Like the plastic case, the contact problem is described by VI.[11] This VI is equivalent to a constrained minimization problem and can be solved by various approximation methods. The penalty method,[11] Lagrange multiplier method,[12] perturbed Lagrangian method,[13] and augmented Lagrangian method[14] are typically used to solve the approximated minimization problem. For a linear problem, it is proven that the projection of the response onto the convex constraint set is directionally differentiable.[15,16] Thus, the solution of VI is directionally differentiable and the derivative is the solution of another VI.[17] When the penalty method is used to approximate the response of VI, it is possible to show that the sensitivity obtained by taking the derivative of approximated variational equation approaches to the solution of the approximated sensitivity VI as the penalty parameter increases.

Without mathematical support, taking the derivative of the approximated variational equation was attempted by several researchers for nonlinear contact problems. Spivey and Tortorelli[18] derived a sensitivity formulation of an elastic beam contact problem with respect to the change of a rigid wall, and Pollock and Noor[19] took derivatives of the finite element equation to compute the sensitivity of the response with respect to dynamic parameters. The sensitivity formulation for the contact problem with respect to the shape perturbation was reported recently by Choi et al.[20] They took derivatives of the contact variational form with respect to the shape

Received 20 June 1999; revision received 20 November 1999; accepted for publication 13 December 1999. Copyright © 2000 by the authors. Published by the American Institute of Aeronautics and Astronautics, Inc., with permission.

*Postdoctoral Associate, Department of Mechanical Engineering and Center for Computer-Aided Design; nkim@ccad.uiowa.edu.

†Professor and Director, Department of Mechanical Engineering and Center for Computer-Aided Design; kkchoi@ccad.uiowa.edu.

‡Associate Professor, Department of Mechanical Engineering and Center for Computer-Aided Design; jschen@icaen.uiowa.edu.

design parameters and used the tangent operator of the sensitivity equation that is consistent with that of the response analysis. The sensitivity equation showed path dependency even for the elastic material because of frictional contact.

During the process of shape design change, the conventional finite element method often has a mesh distortion problem. That is, the regular mesh shape at the original design becomes distorted through the optimum design process, and the reliability of the analysis results is reduced for the new design. The mesh-free methods that were developed recently can be used to relieve the mesh dependence of the analysis. In the mesh-free method, the structural domain is discretized, not by the finite element, but by a set of particles. For a detailed theory and application of the mesh-free method, refer to Ref. 21 and references therein.

In this paper, continuum-based shaped DSA and optimization methods are proposed for the infinitesimal elasto–plasticity with a frictional contact condition. The rate-independent elasto–plasticity is considered with the return mapping algorithm and von Mises yield criterion. The contact condition is formulated using the penalty method and the modified coulomb friction law. The continuum-based shaped design sensitivity for mulation is used for the structural and frictional contact variational equation. The direct differentiation method (DDM) is used to compute the displacement sensitivity and the sensitivity coefficients of various performance measures are computed from the displacement sensitivity. The path dependency of the sensitivity equation from the constitutive relation and friction is discussed. The sensitivities of the stress and internal variables are stored to construct the linear sensitivity equation at the next load step. It is shown that no iteration is required to solve the sensitivity equation. Analysis and the proposed sensitivity formulation are implemented using the mesh-free method. Numerical examples show the accurate results of the proposed method compared to the finite difference method. A design optimization problem for a metal ring contact problem is solved to show the feasibility of proposed method. Difficulties in the sensitivity formulation for the finite deformation elasto–plasticity are also discussed.

II. Variational Principles for Elasto–Plasticity with Contact

A. Rate-Independent Elasto–Plasticity Model

Physically, a plastic deformation can be explained by atomic dislocation. An elastic deformation corresponds to the variation in the interatomic distance without causing atomic dislocation, whereas a plastic deformation implies relative sliding of the atomic layers and a permanent change of the shape without changing the structural volume. A plastic behavior can be efficiently described by the deviator of the tensors, which preserves the volumetric components. The deviatoric stress and strain tensors are defined as

$$\boldsymbol{s} \equiv \boldsymbol{\sigma} - \tfrac{1}{3}\,\mathrm{tr}(\boldsymbol{\sigma})\mathbf{1} = \boldsymbol{I}_{\mathrm{dev}} : \boldsymbol{\sigma} \tag{1}$$

$$\boldsymbol{e} \equiv \varepsilon - \tfrac{1}{3}\,\mathrm{tr}(\varepsilon)\mathbf{1} = \boldsymbol{I}_{\mathrm{dev}} : \varepsilon \tag{2}$$

where $\mathrm{tr}(\bullet)$ is a trace operator, $\mathbf{1}$ is the second-order unit tensor, $\boldsymbol{I}_{\mathrm{dev}} = \boldsymbol{I} - \frac{1}{3}\mathbf{1} \otimes \mathbf{1}$ is the fourth-order unit deviatoric tensor, $\otimes$ is the standard tensor product, $\boldsymbol{I}$ is the fourth-order unit symmetric tensor, and $(:)$ is the contraction operator of tensors.

From the assumption of small elastic strain, the strain and its rate can be additively decomposed into elastic and plastic parts as

$$\varepsilon = \varepsilon^e + \varepsilon^p, \qquad \dot{\varepsilon} = \dot{\varepsilon}^e + \dot{\varepsilon}^p \tag{3}$$

where superscript e and p denote elastic and plastic parts, respectively. For the elastic part, it is usually assumed that there exists an elastic strain energy function such that the stress can be determined by taking a derivative of the elastic energy function with respect to the elastic strain. Here the elastic part is assumed to be linear and

$$W(\varepsilon^e) = \tfrac{1}{2}\varepsilon^e : \boldsymbol{C} : \varepsilon^e = \tfrac{1}{2}(\varepsilon - \varepsilon^p) : \boldsymbol{C} : (\varepsilon - \varepsilon^p) \tag{4}$$

$$\boldsymbol{\sigma} = \frac{\partial W(\varepsilon^e)}{\partial \varepsilon^e} = \boldsymbol{C} : \varepsilon^e = \boldsymbol{C} : (\varepsilon - \varepsilon^p) \tag{5}$$

$$\dot{\boldsymbol{\sigma}} = \boldsymbol{C} : (\dot{\varepsilon} - \dot{\varepsilon}^p) \tag{6}$$

where $\boldsymbol{C} = (\lambda + \frac{2}{3}\mu)\mathbf{1} \otimes \mathbf{1} + 2\mu\boldsymbol{I}_{\mathrm{dev}}$ is the fourth-order isotropic constitutive tensor, and λ and μ are Lame's constants. The rate of stress can be decomposed into volumetric (pressure) and the deviatoric parts from Eq. (6), respectively, as

$$\dot{p} = \tfrac{1}{3}\,\mathrm{tr}(\dot{\boldsymbol{\sigma}}) = \left(\lambda + \tfrac{2}{3}\mu\right)\mathrm{tr}(\dot{\varepsilon}) \tag{7}$$

$$\dot{\boldsymbol{s}} = 2\mu(\dot{\boldsymbol{e}} - \dot{\boldsymbol{e}}^p) \tag{8}$$

For rate independent plasticity, the von Mises pressure insensitive yield criterion with the associative flow rule is the most well-known method used to describe the material behavior after elastic deformation. Accordingly, the yield criterion or yield function is formulated as

$$f(\boldsymbol{\eta}, \hat{e}_p) \equiv \|\boldsymbol{\eta}\| - \sqrt{\tfrac{2}{3}}\kappa(\hat{e}_p) = 0 \tag{9}$$

where $\boldsymbol{\eta} = \boldsymbol{s} - \boldsymbol{\alpha}$, where $\boldsymbol{\alpha}$ is the back stress that is the center of the yield surface (elastic domain) and is determined by the kinematic hardening law, $\kappa(\hat{e}_p)$ is the radius of the elastic domain determined by the isotropic hardening rule, and $\hat{e}_p$ is an effective plastic strain. The combined isotropic/kinematic hardening law is used in Eq. (9). The elastic domain generated by the yield function in Eq. (9) forms a convex set as

$$E = \{(\boldsymbol{\eta}, \hat{e}_p) \mid f(\boldsymbol{\eta}, \hat{e}_p) \le 0\} \tag{10}$$

In mathematical terms, the plasticity can be thought of as a projection of the stress onto the yield surface. Because the yield surface is convex, the projection becomes a contraction mapping, which guarantees the existence of the projection.

It is assumed that there exists a flow potential such that plastic strain is proportional to the normal of the flow potential. If the plastic flow is assumed to be associative, then the flow potential is same as the yield function. Thus,

$$\dot{\boldsymbol{e}}^p = \gamma\frac{\partial f(\boldsymbol{\eta}, \hat{e}_p)}{\partial \boldsymbol{\eta}} = \gamma\frac{\boldsymbol{\eta}}{\|\boldsymbol{\eta}\|} = \gamma\boldsymbol{N} \tag{11}$$

where $\boldsymbol{N}$ is a unit deviatoric tensor and normal to the yield surface and γ is a plastic consistency parameter, which is nonnegative. If the status of material is elastic, γ must be zero, and it is positive for the plastic status. The plastic strain rate is in the direction normal to the yield surface and has the magnitude of plastic consistency parameter γ. As the material experiences plastic deformation, the internal parameter (back stress, effective plastic strain, etc.) is changed by the hardening law. The rate of back stress can be determined by the kinematic hardening law

$$\dot{\boldsymbol{\alpha}} = H_\alpha(\hat{e}_p)\gamma\frac{\partial f(\boldsymbol{\eta}, \hat{e}_p)}{\partial \boldsymbol{\eta}} = H_\alpha(\hat{e}_p)\gamma\boldsymbol{N} \tag{12}$$

where $H_\alpha(\hat{e}_p)$ is the plastic modulus for kinematic hardening. The rate of effective strain can be expressed by

$$\dot{\hat{e}}_p = \sqrt{\tfrac{2}{3}}\left\|\dot{\boldsymbol{e}}^p(t)\right\| = \sqrt{\tfrac{2}{3}}\gamma \tag{13}$$

The Kuhn–Tucker loading/unloading condition becomes

$$\gamma \ge 0, \qquad f \le 0, \qquad \gamma f = 0 \tag{14}$$

The nonpositiveness of the yield function can be thought of as a constraint, and the plastic consistency parameter γ can be thought of as the Lagrange multiplier corresponding to the inequality constraint.

Because all constitutive equations are in rate form in the elasto–plastic model, the calculation of stresses demands integration procedures. The return mapping algorithm is a popular integration procedure. It is well known that the return mapping algorithm, with the radial return method as a special case, is an effective and robust method for rate-independent plasticity.[22] It is assumed that the solution and the status of material at time t_n is known. Because most of the solution procedures of elasto–plasticity problems are of the displacement-driven method, the configuration at time t_{n+1}

is computed using the given displacement. In the return mapping algorithm, a two-step method is often used. At first, the elastic trial status is computed, and if the status of stress is out of the elastic domain, then the trial stress is projected onto the yield surface, which is a convex set. During the projection step, the yield surface itself is changed by the evolution of internal variables.

For associative plasticity, it is well known that the backward Euler method produces the closest point projection. Because the displacement at time t_{n+1} is known for the displacement driven method, the incremental strain at time t_{n+1} can be computed from the definition of the strain. When this incremental strain is used, the first step is called the elastic predictor. The stress and hardening parameters are predicted elastically as

$$ {}^{n+1}\boldsymbol{s}^{\mathrm{tr}} = {}^{n}\boldsymbol{s} + 2\mu\Delta\boldsymbol{e} \tag{15} $$

$$ {}^{n+1}\boldsymbol{\alpha}^{\mathrm{tr}} = {}^{n}\boldsymbol{\alpha} \tag{16} $$

$$ {}^{n+1}\hat{e}_p^{\mathrm{tr}} = {}^{n}\hat{e}_p \tag{17} $$

$$ {}^{n+1}\boldsymbol{\eta}^{\mathrm{tr}} = {}^{n+1}\boldsymbol{s}^{\mathrm{tr}} - {}^{n+1}\boldsymbol{\alpha}^{\mathrm{tr}} \tag{18} $$

where the left-hand superscript $n+1$ denotes the configuration time t_{n+1}.

If the trial stress ${}^{n+1}\eta^{\mathrm{tr}}$ is within the elastic domain, then the stress is updated using the trial predictor and the elastic material status is declared. If the trial stress ${}^{n+1}\eta^{\mathrm{tr}}$ is out of the elastic domain, then the plastic corrector is carried out to find the plastic material status. The stress and hardening parameters are corrected by considering the plastic deformation as

$$ \begin{aligned} {}^{n+1}\boldsymbol{s} &= {}^{n+1}\boldsymbol{s}^{\mathrm{tr}} - 2\mu\Delta\boldsymbol{e}^{p} \\ &= {}^{n+1}\boldsymbol{s}^{\mathrm{tr}} - 2\mu\hat{\gamma}\boldsymbol{N} \end{aligned} \tag{19} $$

$$ {}^{n+1}\boldsymbol{\alpha} = {}^{n+1}\boldsymbol{\alpha}^{\mathrm{tr}} + H_\alpha\hat{\gamma}\boldsymbol{N} \tag{20} $$

$$ \begin{aligned} {}^{n+1}\boldsymbol{\eta} &= {}^{n+1}\boldsymbol{s} - {}^{n+1}\boldsymbol{\alpha} \\ &= {}^{n+1}\boldsymbol{\eta}^{\mathrm{tr}} - (2\mu + H_\alpha)\hat{\gamma}\boldsymbol{N} \end{aligned} \tag{21} $$

where $\boldsymbol{N} = {}^{n+1}\boldsymbol{\eta}/\|{}^{n+1}\boldsymbol{\eta}\|$, which is a unit deviatoric tensor and normal to the yield function at time t_{n+1}, and where $\hat{\gamma} = \gamma\Delta t$ is computed from the yield condition at time t_{n+1}. An important feature of Eq. (21) is that the trial stress is in the same direction as the final stress. Thus, the unit normal tensor to the yield surface can be computed from the trial stress by

$$ \boldsymbol{N} = \frac{{}^{n+1}\boldsymbol{\eta}^{\mathrm{tr}}}{\|{}^{n+1}\boldsymbol{\eta}^{\mathrm{tr}}\|} \tag{22} $$

which is known from the elastic predictor step.

At the return map point the following yield condition is satisfied:

$$ \begin{aligned} f\left({}^{n+1}\boldsymbol{\eta}, {}^{n+1}\hat{e}_p\right) &= \|{}^{n+1}\boldsymbol{\eta}\| - \sqrt{\tfrac{2}{3}}\kappa\left({}^{n+1}\hat{e}_p\right) \\ &= \|{}^{n+1}\boldsymbol{\eta}^{\mathrm{tr}}\| - \left[2\mu + H_\alpha\left({}^{n+1}\hat{e}_p\right)\right]\hat{\gamma} - \sqrt{\tfrac{2}{3}}\kappa\left({}^{n+1}\hat{e}_p\right) = 0 \end{aligned} \tag{23} $$

which is a nonlinear equation in terms of $\hat{\gamma}$. Equation (23) can be solved to compute $\hat{\gamma}$ using the local Newton method. If the isotropic/kinematic hardening is a linear function of $\hat{\gamma}$ or the effective plastic strain, then only one iteration is required to compute the return map point. After $\hat{\gamma}$ is found, the stress and hardening parameters can be updated at time t_{n+1} by

$$ {}^{n+1}\boldsymbol{s} = {}^{n}\boldsymbol{s} + 2\mu\Delta\boldsymbol{e} - 2\mu\hat{\gamma}\boldsymbol{N} \tag{24} $$

$$ {}^{n+1}\boldsymbol{\sigma} = {}^{n}\boldsymbol{\sigma} + \Delta\boldsymbol{\sigma} \tag{25} $$

$$ \Delta\boldsymbol{\sigma} = \boldsymbol{C} : \Delta\varepsilon - 2\mu\hat{\gamma}\boldsymbol{N} \tag{26} $$

$$ {}^{n+1}\boldsymbol{\alpha} = {}^{n}\boldsymbol{\alpha} + H_\alpha\hat{\gamma}\boldsymbol{N} \tag{27} $$

$$ {}^{n+1}\hat{e}_p = {}^{n}\hat{e}_p + \sqrt{\tfrac{2}{3}}\hat{\gamma} \tag{28} $$

As discussed by Simo and Taylor,[4] the tangent operator must be consistent with the time integration algorithm to achieve quadratic convergence of the Newton method. The differentiation of the incremental stress tensor in Eq. (26) is taken with respect to the incremental strain tensor, which produces a consistent constitutive relation with the return mapping algorithm. Thus, the consistent or algorithmic tangent operator becomes

$$ \boldsymbol{C}^{\mathrm{alg}} = \frac{\partial\Delta\boldsymbol{\sigma}}{\partial\Delta\varepsilon} = \boldsymbol{C} - 4\mu^2 A\boldsymbol{N}\otimes\boldsymbol{N} - \frac{4\mu^2\hat{\gamma}}{\|{}^{n+1}\boldsymbol{\eta}^{\mathrm{tr}}\|}[\boldsymbol{I}_{\mathrm{dev}} - \boldsymbol{N}\otimes\boldsymbol{N}] \tag{29} $$

where $A \equiv 1/(2\mu + H_\alpha + \sqrt{\frac{2}{3}}H'_\alpha\hat{\gamma} + \frac{2}{3}\kappa')$, $\kappa' = \partial\kappa/\partial\hat{e}_p$ and $H'_\alpha = \partial H_\alpha/\partial\hat{e}_p$. For a notational convenience, define the structural energy form and its linearization by

$$ a_\Omega({}^{n+1}z, \bar{z}) \equiv \int_\Omega \varepsilon(\bar{z}) : {}^{n+1}\boldsymbol{\sigma}\, d\Omega \tag{30} $$

$$ a^*_\Omega({}^{n}z; \Delta z, \bar{z}) \equiv \int_\Omega \varepsilon(\bar{z}) : \boldsymbol{C}^{\mathrm{alg}} : \varepsilon(\Delta z)\, d\Omega \tag{31} $$

B. Frictional Contact with a Rigid Wall

In this section, the contact variational form is derived based on the continuum formulation. For details, refer to Ref. 20. Figure 1 shows a general contact condition with a rigid wall in R^2. Because the motion of the rigid wall is fixed or prescribed throughout the analysis, a natural coordinate or parameter ξ can represent the surface coordinate of the rigid wall. The coordinate of contact point $\boldsymbol{x}_c$ can be represented using a natural coordinate at the contact point ξ_c by $\boldsymbol{x}_c = \boldsymbol{x}_c(\xi_c)$. The normal contact condition can be imposed on the structure by measuring the distance between a part of the structural boundary Γ_c and the surface of the rigid wall. An impenetration condition can be defined, using the normal gap function g_n, that measures the normal distance as

$$ g_n \equiv [\boldsymbol{x} - \boldsymbol{x}_c(\xi_c)]^T\boldsymbol{e}_n(\xi_c) \geq 0, \qquad \boldsymbol{x} \in \Gamma_c \tag{32} $$

where $\boldsymbol{e}_n$ is the unit outward normal vector of the rigid wall at the contact point. The contact point $\boldsymbol{x}_c$ that corresponds to the body point $\boldsymbol{x} \in \Gamma_c$ is determined by solving the following nonlinear equation:

$$ \varphi(\xi_c) = [\boldsymbol{x} - \boldsymbol{x}_c(\xi_c)]^T\boldsymbol{e}_t(\xi_c) = 0 \tag{33} $$

where $\boldsymbol{e}_t$ is the unit tangential vector at the contact point. Equation (33) is called a contact consistency condition. In Eq. (33), $\boldsymbol{x}_c(\xi_c)$ is the closest projection point of $\boldsymbol{x} \in \Gamma_c$ onto the rigid wall by imposing the contact consistency condition.

As the contact point moves along the rigid wall, there exists a frictional force along the tangential direction of the rigid wall that resists the tangential relative movement. Tangential slip function g_t is the measure of the relative movement of the contact point along

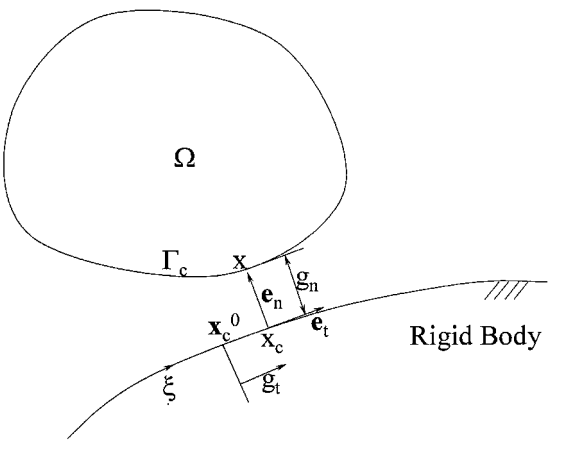

Fig. 1 Continuum-based frictional contact condition in R^2.

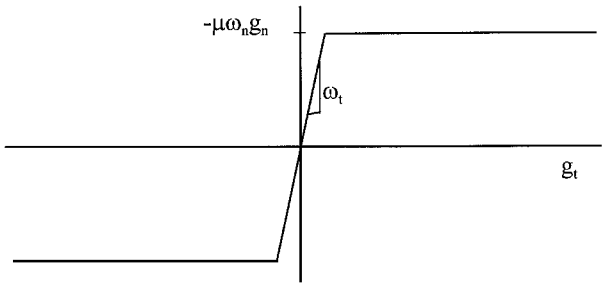

Fig. 2 Modified coulomb friction model.

the rigid wall,

$$g_t \equiv \|\boldsymbol{t}^0\|\left(\xi_c - \xi_c^0\right) \tag{34}$$

where $\|\boldsymbol{t}^0\|$ is the norm of the tangential vector and ξ_c^0 is the natural coordinate of the earlier converged time step. For the convenience of the following derivations, define several scalar symbols:

$$\alpha \equiv \boldsymbol{e}_n^T \boldsymbol{x}_{c,\xi\xi}, \qquad \beta \equiv \boldsymbol{e}_t^T \boldsymbol{x}_{c,\xi\xi}, \qquad \gamma \equiv \boldsymbol{e}_n^T \boldsymbol{x}_{c,\xi\xi\xi}$$
$$c \equiv \|\boldsymbol{t}\|^2 - g_n\alpha, \qquad \nu \equiv \|\boldsymbol{t}\|\|\boldsymbol{t}^0\|/c \tag{35}$$

The frictional force is bounded above by $-\mu\,\omega_n g_n$ in the coulomb friction law. However, for the case of small slip (microdisplacement), the traction force is proportional to the tangential slip. The penalty parameter ω_t is a constant for this case. Figure 2 shows a friction curve used in this paper. A stick condition occurs when the frictional traction force is less than the normal force multiplied by the frictional coefficient as

$$|\omega_t g_t| \le |\mu\,\omega_n g_n| \tag{36}$$

Otherwise, it becomes a slip condition. In Eq. (36), μ is the coulomb friction coefficient. Thus, the contact variational form can be classified as either the stick condition or the slip condition. From the standard penalty formulation,

$$b(\boldsymbol{z},\bar{\boldsymbol{z}}) = \omega_n \int_{\Gamma_C} g_n \bar{\boldsymbol{z}}^T \boldsymbol{e}_n \,\mathrm{d}\Gamma$$
$$+ \begin{cases} +\omega_t \displaystyle\int_{\Gamma_C} \nu g_t \bar{\boldsymbol{z}}^T \boldsymbol{e}_t \,\mathrm{d}\Gamma & \text{if} \quad |\omega_t g_t| \le |\mu\,\omega_n g_n| \\ -\mu\,\omega_n \operatorname{sgn}(g_t) \displaystyle\int_{\Gamma_C} \nu g_n \bar{\boldsymbol{z}}^T \boldsymbol{e}_t \,\mathrm{d}\Gamma & \text{otherwise} \end{cases}$$
$$\equiv b_N(\boldsymbol{z},\bar{\boldsymbol{z}}) + b_T(\boldsymbol{z},\bar{\boldsymbol{z}}) \tag{37}$$

where $b_N(\boldsymbol{z},\bar{\boldsymbol{z}})$ is the normal contact variational form and $b_T(\boldsymbol{z},\bar{\boldsymbol{z}})$ is the tangential stick/slip variational form. The contact variational form in Eq. (37) is a nonlinear relation with respect to the displacement. The linearization of a normal contact variational form in Eq. (30) leads to the linearized normal contact variational form

$$b_N^*({}^n\boldsymbol{z};\Delta\boldsymbol{z},\bar{\boldsymbol{z}})$$
$$= \omega_n \int_{\Gamma_C} \bar{\boldsymbol{z}}^{T\,n} \boldsymbol{e}_n^n \boldsymbol{e}_n^{\,T} \Delta\boldsymbol{z}\,\mathrm{d}\Gamma - \omega_n \int_{\Gamma_C}^{n} \frac{\alpha g_n}{c} \bar{\boldsymbol{z}}^{T\,n} \boldsymbol{e}_t^n \boldsymbol{e}_t^{\,T} \Delta\boldsymbol{z}\,\mathrm{d}\Gamma \tag{38}$$

Note that in Eq. (38) there is a component in the tangential direction because of the curvature effects.

The linearization of the tangential stick condition leads to the linearized tangential stick variational form

$$b_T^*({}^n\boldsymbol{z};\Delta\boldsymbol{z},\bar{\boldsymbol{z}}) = \omega_t \int_{\Gamma_C} \nu^2 \bar{\boldsymbol{z}}^{T\,n} \boldsymbol{e}_t^n \boldsymbol{e}_t^{\,T} \Delta\boldsymbol{z}\,\mathrm{d}\Gamma$$
$$+ \omega_t \int_{\Gamma_C}^{n} \frac{\alpha \nu g_t}{c} \bar{\boldsymbol{z}}^T \left({}^n\boldsymbol{e}_n^n \boldsymbol{e}_t + {}^n\boldsymbol{e}_t^n \boldsymbol{e}_n\right)^T \Delta\boldsymbol{z}\,\mathrm{d}\Gamma$$
$$+ \omega_t \int_{\Gamma_C}^{n} \left(\frac{\nu g_t}{c^2}\right)^n \left[(\gamma\|\boldsymbol{t}\| - 2\alpha\beta)g_n - \beta\|\boldsymbol{t}\|^2\right] \bar{\boldsymbol{z}}^{T\,n} \boldsymbol{e}_t^n \boldsymbol{e}_t^{\,T} \Delta\boldsymbol{z}\,\mathrm{d}\Gamma \tag{39}$$

and the linearization of the tangential slip condition leads to the linearized tangential slip variational form

$$b_T^*({}^n\boldsymbol{z};\Delta\boldsymbol{z},\bar{\boldsymbol{z}}) = \omega_t \int_{\Gamma_C}^{n} \nu \bar{\boldsymbol{z}}^{T\,n} \boldsymbol{e}_t^n \boldsymbol{e}_n^{\,T} \Delta\boldsymbol{z}\,\mathrm{d}\Gamma$$
$$+ \omega_t \int_{\Gamma_C}^{n} \frac{\alpha \nu g_n}{c} \bar{\boldsymbol{z}}^T \left({}^n\boldsymbol{e}_n^n \boldsymbol{e}_t^T + {}^n\boldsymbol{e}_t^n \boldsymbol{e}_n^T\right) \Delta\boldsymbol{z}\,\mathrm{d}\Gamma$$
$$+ \omega_t \int_{\Gamma_C}^{n} \left(\frac{\nu g_n}{c^2}\right)^n \left[(\gamma\|\boldsymbol{t}\| - 2\alpha\beta)g_n - \beta\|\boldsymbol{t}\|^2\right] \bar{\boldsymbol{z}}^{T\,n} \boldsymbol{e}_t^n \boldsymbol{e}_t^{\,T} \Delta\boldsymbol{z}\,\mathrm{d}\Gamma \tag{40}$$

where, for the case of the slip contact condition, the tangential penalty parameter ω_t is related to normal penalty parameter ω_n by

$$\omega_t = -\mu\,\omega_n \operatorname{sgn}(g_t) \tag{41}$$

The linearized contact variational form is the sum of Eqs. (38) and (39) [or Eq. (40)] as

$$b_\Gamma^*({}^n\boldsymbol{z};\Delta\boldsymbol{z},\bar{\boldsymbol{z}}) = b_N^*({}^n\boldsymbol{z};\Delta\boldsymbol{z},\bar{\boldsymbol{z}}) + b_T^*({}^n\boldsymbol{z};\Delta\boldsymbol{z},\bar{\boldsymbol{z}}) \tag{42}$$

For the case of the stick condition, the linearized contact variational form Eq. (42) is symmetric bilinear with respect to the incremental displacement and the variation of displacement. This is expected because the contact phenomena for a stick condition are elastic. For the case of the slip condition, the linearized contact variational form Eq. (42) is not symmetric with respect to incremental displacement and the variation of displacement. The system is no longer conservative if it starts to slip along the master surface.

C. Variational Principles for Elasto-Plasticity with Contact

Suppose that the solution and configurations of the problem up to time t_n are known, and the solution and configurations at time t_{n+1} are required. The variational equation at time t_{n+1} can be written as

$$a_\Omega({}^{n+1}\boldsymbol{z},\bar{\boldsymbol{z}}) + b_\Gamma({}^{n+1}\boldsymbol{z},\bar{\boldsymbol{z}}) = \ell_\Omega(\bar{\boldsymbol{z}}), \qquad \forall \bar{\boldsymbol{z}} \in Z \tag{43}$$

where Z is the space of the kinematically admissible displacement and

$$\ell_\Omega(\bar{\boldsymbol{z}}) = \int_\Omega \bar{\boldsymbol{z}}^{T\,n+1} \boldsymbol{f}^B \,\mathrm{d}\Omega + \int_{\Gamma_T} \bar{\boldsymbol{z}}^{T\,n+1} \boldsymbol{f}^T \,\mathrm{d}\Gamma \tag{44}$$

is the load linear form and is assumed to be independent of the deformation. Equation (43) is a nonlinear function of displacement and is linearized with respect to incremental displacement and then solved iteratively using the Newton method. Let the current time be t_{n+1}, and let k be the last iteration counter. Then the incremental equation of Eq. (43) can be written as

$$a_\Omega^*({}^{n+1}\boldsymbol{z}^k;\Delta\boldsymbol{z}^{k+1},\bar{\boldsymbol{z}}) + b_\Gamma^*({}^{n+1}\boldsymbol{z}^k;\Delta\boldsymbol{z}^{k+1},\bar{\boldsymbol{z}})$$
$$= \ell_\Omega(\bar{\boldsymbol{z}}) - a_\Omega({}^{n+1}\boldsymbol{z}^k,\bar{\boldsymbol{z}}) - b_\Gamma({}^{n+1}\boldsymbol{z}^k,\bar{\boldsymbol{z}}), \qquad \forall \bar{\boldsymbol{z}} \in Z \tag{45}$$

The incremental Eq. (45) is solved iteratively until the residual terms (right-hand side) vanish. When the variational equation is converged, the tangent stiffness matrix (left-hand side) is stored so that it can be used at the DSA procedure.

III. Shape Design Sensitivity Formulation

A. Shape DSA of Elasto-Plasticity

The shape DSA starts with defining the design velocity field, which is the direction of the design perturbation and is assumed to be given. The perturbation of the geometry in the direction of the design velocity field $\boldsymbol{V}(\boldsymbol{x})$ is controlled by a parameter τ (Fig. 3). The material derivative of displacement $\boldsymbol{z}(\boldsymbol{x})$ is defined as

$$\dot{\boldsymbol{z}} = \lim_{\tau\to 0} \left\{\frac{\boldsymbol{z}_\tau[\boldsymbol{x} + \tau\boldsymbol{V}(\boldsymbol{x})] - \boldsymbol{z}(\boldsymbol{x})}{\tau}\right\}$$
$$= \boldsymbol{z}' + \nabla\boldsymbol{z}^T\boldsymbol{V} \tag{46}$$

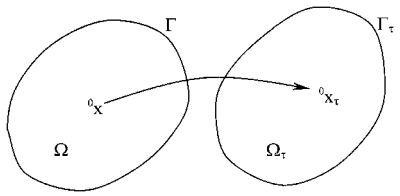

Fig. 3 Variation of undeformed domain by one-parameter family of mappings.

where

$$z' = \lim_{\tau \to 0}\left[\frac{z_\tau(\boldsymbol{x}) - z(\boldsymbol{x})}{\tau}\right] \tag{47}$$

is the partial derivative of z. For a rigorous definition of the perturbation and the material derivative, refer to Ref. 1, Chapter 3.

The governing variational equation of plasticity with contact at the perturbed design is

$$a_{\Omega_\tau}\left({}^{n+1}z_\tau, \bar{z}_\tau\right) + b_{\Gamma_\tau}\left({}^{n+1}z_\tau, \bar{z}_\tau\right) = \ell_{\Omega_\tau}(\bar{z}_\tau), \qquad \forall \bar{z}_\tau \in Z_\tau \tag{48}$$

where Z_τ is the space of the kinematically admissible displacements at the perturbed design.

For the elasto–plastic material, the constitutive relation is given by incremental form

$${}^{n+1}\boldsymbol{\sigma} = {}^{n}\boldsymbol{\sigma} + \boldsymbol{C} : (\Delta\varepsilon - \Delta\varepsilon^p) \tag{49}$$

Thus, the material derivative of the stress tensor includes that of the incremental strain. Because of the small deformation assumption, it can be shown that

$$\frac{\mathrm{d}}{\mathrm{d}\tau}(\Delta\varepsilon) = \frac{1}{2}[\nabla(\Delta\dot{z}) + \nabla(\Delta\dot{z})^T] - \frac{1}{2}[\nabla(\Delta z)\nabla\boldsymbol{V} + \nabla\boldsymbol{V}^T\nabla(\Delta z)^T]$$
$$\equiv \varepsilon(\Delta\dot{z}) + \varepsilon_V(\Delta z) \tag{50}$$

$$\frac{\mathrm{d}}{\mathrm{d}\tau}[\varepsilon(\bar{z})] = -\frac{1}{2}(\nabla\bar{z}\nabla\boldsymbol{V} + \nabla\boldsymbol{V}^T\nabla\bar{z}^T) \equiv \varepsilon_V(\bar{z}) \tag{51}$$

Because $\dot{\bar{z}}$ is in the same space as $\bar{z}$, all of the terms containing $\dot{\bar{z}}$ are ignored in Eq. (51) in the sense of $a_\Omega({}^{n+1}z, \dot{\bar{z}}) + b_\Gamma({}^{n+1}z, \dot{\bar{z}}) = \ell_\Omega(\dot{\bar{z}})$. Note that the material derivative of the incremental strain has the same structure as the total strain by substituting $\Delta\dot{z}$ into Δz because the kinematics are linear even if the constitutive relation is nonlinear. This is not true for the case of a nonlinear kinematic relation where the sensitivity of the incremental strain has a different structure from the total strain.

The sensitivity of the stress tensor can be obtained by taking the derivative of the return mapping algorithm consistently with response analysis. Sensitivities of the internal evolution variables are also computed the same way. Consider when the material is in the elastic status. The Cauchy stress is increased elastically and internal variables remain constant through the deformation as

$$\frac{\mathrm{d}}{\mathrm{d}\tau}({}^{n+1}\boldsymbol{\sigma}) = \frac{\mathrm{d}}{\mathrm{d}\tau}({}^{n}\boldsymbol{\sigma}) + \boldsymbol{C} : \frac{\mathrm{d}}{\mathrm{d}\tau}(\Delta\varepsilon)$$
$$= \frac{\mathrm{d}}{\mathrm{d}\tau}({}^{n}\boldsymbol{\sigma}) + \boldsymbol{C} : \varepsilon(\Delta\dot{z}) + \boldsymbol{C} : \varepsilon_V(\Delta z) \tag{52}$$

$$\frac{\mathrm{d}}{\mathrm{d}\tau}({}^{n+1}\boldsymbol{\alpha}) = \frac{\mathrm{d}}{\mathrm{d}\tau}({}^{n}\boldsymbol{\alpha}) \tag{53}$$

$$\frac{\mathrm{d}}{\mathrm{d}\tau}\left({}^{n+1}\hat{e}_p\right) = \frac{\mathrm{d}}{\mathrm{d}\tau}\left({}^{n}\hat{e}_p\right) \tag{54}$$

However, when the material is in the plastic stage, the material derivative of the stress and internal variables follow the return mapping algorithm. The material derivative formulas for the elastic trial status are

$$\frac{\mathrm{d}}{\mathrm{d}\tau}({}^{n+1}\boldsymbol{s}^{\mathrm{tr}}) = \frac{\mathrm{d}}{\mathrm{d}\tau}({}^{n}\boldsymbol{s}) + 2\mu\frac{\mathrm{d}}{\mathrm{d}\tau}(\Delta\boldsymbol{e}) \tag{55}$$

$$\frac{\mathrm{d}}{\mathrm{d}\tau}({}^{n+1}\boldsymbol{\alpha}^{\mathrm{tr}}) = \frac{\mathrm{d}}{\mathrm{d}\tau}({}^{n}\boldsymbol{\alpha}) \tag{56}$$

$$\frac{\mathrm{d}}{\mathrm{d}\tau}\left({}^{n+1}\hat{e}_p^{\mathrm{tr}}\right) = \frac{\mathrm{d}}{\mathrm{d}\tau}\left({}^{n}\hat{e}_p\right) \tag{57}$$

$$\frac{\mathrm{d}}{\mathrm{d}\tau}({}^{n+1}\boldsymbol{\eta}^{\mathrm{tr}}) = \frac{\mathrm{d}}{\mathrm{d}\tau}({}^{n+1}\boldsymbol{s}^{\mathrm{tr}}) - \frac{\mathrm{d}}{\mathrm{d}\tau}({}^{n+1}\boldsymbol{\alpha}^{\mathrm{tr}})$$
$$= \frac{\mathrm{d}}{\mathrm{d}\tau}({}^{n}\boldsymbol{\eta}) + 2\mu\frac{\mathrm{d}}{\mathrm{d}\tau}(\Delta\boldsymbol{e}) \tag{58}$$

If the von Mises yield criterion is used with an associative plasticity assumption, the return mapping direction is radial, and the normal of the trial stress is the same as that of the final stress. The material derivative of the normal tensor in Eq. (22) becomes

$$\frac{\mathrm{d}}{\mathrm{d}\tau}(\boldsymbol{N}) = \frac{2\mu}{\|{}^{n+1}\boldsymbol{\eta}^{\mathrm{tr}}\|}[\boldsymbol{I} - \boldsymbol{N}\otimes\boldsymbol{N}] : \frac{\mathrm{d}}{\mathrm{d}\tau}(\Delta\boldsymbol{e})$$
$$+ \frac{1}{\|{}^{n+1}\boldsymbol{\eta}^{\mathrm{tr}}\|}[\boldsymbol{I} - \boldsymbol{N}\otimes\boldsymbol{N}] : \frac{\mathrm{d}}{\mathrm{d}\tau}({}^{n}\boldsymbol{\eta}) \tag{59}$$

The radial return mapping algorithm is computing the plastic consistency parameter $\hat{\gamma}$ through the plastic consistency condition. The material derivative of the plastic consistency condition Eq. (23) is

$$\frac{\mathrm{d}}{\mathrm{d}\tau}(f) = \frac{\mathrm{d}}{\mathrm{d}\tau}\|{}^{n+1}\boldsymbol{\eta}^{\mathrm{tr}}\| - \frac{\mathrm{d}}{\mathrm{d}\tau}\left[(2\mu + H_\alpha)\hat{\gamma} + \sqrt{\frac{2}{3}}\kappa\left({}^{n+1}\hat{e}_p\right)\right] = 0 \tag{60}$$

By solving this equation in terms of $\mathrm{d}/\mathrm{d}\tau(\hat{\gamma})$, it can be shown that

$$\frac{\mathrm{d}}{\mathrm{d}\tau}(\hat{\gamma}) = 2\mu\boldsymbol{A}\boldsymbol{N} : \frac{\mathrm{d}}{\mathrm{d}\tau}(\Delta\boldsymbol{e})$$
$$+ \boldsymbol{A}\boldsymbol{N} : \frac{\mathrm{d}}{\mathrm{d}\tau}({}^{n}\boldsymbol{\eta}) - A\left(H'_\alpha\hat{\gamma} + \sqrt{\frac{2}{3}}\kappa'\right)\frac{\mathrm{d}}{\mathrm{d}\tau}\left({}^{n}\hat{e}_p\right) \tag{61}$$

Note that there is no iteration to compute $\mathrm{d}/\mathrm{d}\tau(\hat{\gamma})$ in Eq. (61), whereas analysis is carried out iteratively to compute $\hat{\gamma}$ using the local Newton method. By taking a derivative of the stress updating algorithm Eqs. (25) and (26), the material derivative of Cauchy stress can be obtained as

$$\frac{\mathrm{d}}{\mathrm{d}\tau}({}^{n+1}\boldsymbol{\sigma}) = \frac{\mathrm{d}}{\mathrm{d}\tau}({}^{n}\boldsymbol{\sigma}) + \boldsymbol{C} : \frac{\mathrm{d}}{\mathrm{d}\tau}(\Delta\varepsilon) - 2\mu\boldsymbol{N}\frac{\mathrm{d}}{\mathrm{d}\tau}(\hat{\gamma}) - 2\mu\hat{\gamma}\frac{\mathrm{d}}{\mathrm{d}\tau}(\boldsymbol{N})$$
$$= \boldsymbol{C}^{\mathrm{alg}} : \varepsilon(\Delta\dot{z}) + \boldsymbol{C}^{\mathrm{alg}} : \varepsilon_V(\Delta z) + {}^{n+1}\boldsymbol{\sigma}^{\mathrm{fic}} \tag{62}$$

where

$${}^{n+1}\boldsymbol{\sigma}^{\mathrm{fic}} = \frac{\mathrm{d}}{\mathrm{d}\tau}({}^{n}\boldsymbol{\sigma}) - 2\mu\boldsymbol{A}\boldsymbol{N}$$
$$\times\left[\boldsymbol{N} : \frac{\mathrm{d}}{\mathrm{d}\tau}({}^{n}\boldsymbol{\eta}) - \left(H'_\alpha\hat{\gamma} + \sqrt{\frac{2}{3}}\kappa'\right)\frac{\mathrm{d}}{\mathrm{d}\tau}\left({}^{n}\hat{e}_p\right)\right]$$
$$- \frac{2\mu\hat{\gamma}}{\|{}^{n+1}\boldsymbol{\eta}^{\mathrm{tr}}\|}(\boldsymbol{I} - \boldsymbol{N}\otimes\boldsymbol{N})\frac{\mathrm{d}}{\mathrm{d}\tau}({}^{n}\boldsymbol{\eta}) \tag{63}$$

can be computed from the information at time t_n and the trial status, and $\boldsymbol{C}^{\mathrm{alg}} : \varepsilon_V(\Delta z)$ are computed using given design velocity field $\boldsymbol{V}$ and the response Δz.

By using stress sensitivity in Eq. (62), the derivative of the structural energy form in Eq. (43) can be obtained as

$$\frac{\mathrm{d}}{\mathrm{d}\tau}\left[a_\Omega({}^{n+1}z, \bar{z})\right] = a^*_\Omega({}^{n+1}z, \Delta\dot{z}, \bar{z}) + a'_V({}^{n+1}z, \bar{z}) \tag{64}$$

where

$$a'_V({}^{n+1}z, \bar{z}) = \int_\Omega \left[\varepsilon_V(\bar{z}) : {}^{n+1}\boldsymbol{\sigma} + \varepsilon(\bar{z}) : \boldsymbol{C}^{\mathrm{alg}} : \varepsilon_V(\Delta z)\right.$$
$$\left. + \varepsilon(\bar{z}) : {}^{n+1}\boldsymbol{\sigma}^{\mathrm{fic}} + \varepsilon(\bar{z}) : {}^{n+1}\boldsymbol{\sigma}(\mathrm{div}\boldsymbol{V})\right]\mathrm{d}\Omega \tag{65}$$

is the structural fictitious load form and can be obtained using the design velocity field $\boldsymbol{V}(\boldsymbol{x})$ and response ${}^{n+1}z$.

B. Shape DSA of the Contact Problem

The material derivative of structural point ${}^{n+1}\boldsymbol{x} \in {}^{n+1}\Omega$ at time t_{n+1} becomes

$$\frac{\mathrm{d}}{\mathrm{d}\tau}({}^{n+1}\boldsymbol{x}) \equiv \frac{\mathrm{d}}{\mathrm{d}\tau}({}^{0}\boldsymbol{x} + {}^{n+1}z) = \boldsymbol{V}({}^{0}\boldsymbol{x}) + {}^{n}\dot{z} + \Delta\dot{z} \tag{66}$$

Because the derivative of the structural variational form is expressed in terms of the derivative of the incremental displacement, $\Delta\dot{z}$ is explicitly denoted in Eq. (66). However, the perturbation of the contact point ${}^{n+1}\boldsymbol{x}_c$ on the master surface Γ_c can be obtained by using the perturbation of the natural coordinate corresponding to the contact point to the tangential direction as

$$\frac{\mathrm{d}}{\mathrm{d}\tau}\left({}^{n+1}\boldsymbol{x}_c\right) = {}^{n+1}\boldsymbol{t}\frac{\mathrm{d}}{\mathrm{d}\tau}\left({}^{n+1}\xi_c\right) \tag{67}$$

The contact variational form in Eq. (37) is differentiated with respect to the design perturbation at the original geometry to construct the DSA equation. For detailed derivations of the following, refer to Ref. 20. The material derivative formulas of the unit tangent/normal vectors and normal gap/tangential slip functions can be obtained from their definitions as

$$\frac{\mathrm{d}}{\mathrm{d}\tau}\left({}^{n+1}\boldsymbol{e}_t\right) = \frac{{}^{n+1}\alpha}{{}^{n+1}c}\left[(\boldsymbol{V} + {}^{n+1}\dot{z})^{T\,n+1}\boldsymbol{e}_t\right]{}^{n+1}\boldsymbol{e}_n \tag{68}$$

$$\frac{\mathrm{d}}{\mathrm{d}\tau}\left({}^{n+1}\boldsymbol{e}_n\right) = -\frac{{}^{n+1}\alpha}{{}^{n+1}c}\left[(\boldsymbol{V} + {}^{n+1}\dot{z})^{T\,n+1}\boldsymbol{e}_t\right]{}^{n+1}\boldsymbol{e}_t \tag{69}$$

$$\frac{\mathrm{d}}{\mathrm{d}\tau}\left({}^{n+1}g_n\right) = \frac{\mathrm{d}}{\mathrm{d}\tau}\left[\left({}^{n+1}\boldsymbol{x} - {}^{n+1}\boldsymbol{x}_c\right)^{T\,n+1}\boldsymbol{e}_n\right] = (\boldsymbol{V} + {}^{n+1}\dot{z})^{T\,n+1}\boldsymbol{e}_n \tag{70}$$

$$\frac{\mathrm{d}}{\mathrm{d}\tau}\left({}^{n+1}g_t\right) = {}^{n+1}\nu^{n+1}\boldsymbol{e}_t^T(\boldsymbol{V} + {}^{n+1}\dot{z}) + \frac{{}^{n}\beta^{n+1}g_t - \|{}^{n}\boldsymbol{t}\|^2}{{}^{n}c}{}^{n}\boldsymbol{e}_t^T(\boldsymbol{V} + {}^{n}\dot{z}) \tag{71}$$

where the derivative of the contact consistency condition in Eq. (33) is used to compute the derivative of the contact consistency parameter $\mathrm{d}/\mathrm{d}\tau({}^{n+1}\xi_c)$. The derivative of the tangential slip function at time t_{n+1} depends on the derivative of the displacement at time t_n, which makes the problem a path-dependent one.

If the rigid wall is piecewise linear and the movement of the rigid wall is fixed or prescribed, then Eqs. (68) and (69) become zero because the second derivative of the rigid wall with respect to the natural coordinate ξ is zero. Many analysis programs use contact algorithms between slave nodes and linear master segments. In that case, Eqs. (68) and (69) can be ignored. However, for the case of a general rigid wall or a multibody contact problem, the unit normal vector $\boldsymbol{e}_n$ and the tangential vector $\boldsymbol{e}_t$ may change along with the shape change. It is necessary to evaluate the derivative of the unit normal and tangential vectors of the rigid wall from Eqs. (68) and (69).

The material derivative of the normal contact variational form in Eq. (37) becomes

$$\frac{\mathrm{d}}{\mathrm{d}\tau}\left[b_N({}^{n+1}z, \bar{z})\right] \equiv b_N^*({}^{n+1}z; \Delta\dot{z}, \bar{z}) + b_N'({}^{n+1}z, \bar{z}) \tag{72}$$

where

$$b_N'({}^{n+1}z, \bar{z}) = b_N^*({}^{n+1}z; \boldsymbol{V} + {}^{n}\dot{z}, \bar{z}) + \omega_n \int_{\Gamma_C} \kappa\left({}^{n+1}g_n{}^{n+1}\boldsymbol{e}_n^T\bar{z}\right)\boldsymbol{V}^T\boldsymbol{n}\,\mathrm{d}\Gamma \tag{73}$$

is the normal contact fictitious load form and κ is the curvature of the contact boundary.

The material derivative of the tangential stick/slip variational form in Eq. (37) with respect to shape design becomes

$$\frac{\mathrm{d}}{\mathrm{d}\tau}\left[b_T({}^{n+1}z, \bar{z})\right] \equiv b_T^*({}^{n+1}z; \Delta\dot{z}, \bar{z}) + b_T'({}^{n+1}z, \bar{z}) \tag{74}$$

where $b_T^*({}^{n+1}z; \Delta\dot{z}, \bar{z})$ is obtained from the linearized tangential stick/slip variational form in Eq. (39) or (40) by replacing Δz with $\Delta\dot{z}$ and

$$b_T'({}^{n+1}z, \bar{z}) = b_T^*({}^{n+1}z; \boldsymbol{V} + {}^{n}\dot{z}, \bar{z}) + \omega_t \int_{\Gamma_C} \left(2^{n+1}\nu^n\beta^{n+1}g_t - {}^{n+1}\nu\|{}^{n}\boldsymbol{t}\|^2\right)\bar{z}^{T\,n+1}\boldsymbol{e}_t^n\boldsymbol{e}_t^T(\boldsymbol{V} + {}^{n}\dot{z})\,\mathrm{d}\Gamma + \omega_t \int_{\Gamma_C} \kappa^{n+1}\nu^{n+1}g_t\bar{z}^{T\,n+1}\boldsymbol{e}_t(\boldsymbol{V}^T\boldsymbol{n})\,\mathrm{d}\Gamma \tag{75}$$

is the tangential stick fictitious load form for the case of the stick condition and

$$b_T'({}^{n+1}z, \bar{z}) \equiv b_T^*({}^{n+1}z; \boldsymbol{V} + {}^{n}\dot{z}, \bar{z}) + \omega_t \int_{\Gamma_C} \frac{{}^{n+1}\nu^n\beta^{n+1}g_n}{{}^{n}c}\bar{z}^{T\,n+1}\boldsymbol{e}_t^n\boldsymbol{e}_t^T(\boldsymbol{V} + {}^{n}\dot{z})\,\mathrm{d}\Gamma + \omega_t \int_{\Gamma_C} \kappa^{n+1}\nu^{n+1}g_n\bar{z}^{T\,n+1}\boldsymbol{e}_t(\boldsymbol{V}^T\boldsymbol{n})\,\mathrm{d}\Gamma \tag{76}$$

is the tangential slip fictitious load form for the case of the slip condition, respectively. Note that the same symbol of $b_T'({}^{n+1}z, \bar{z})$ is used for both stick and slip conditions. Thus, the material derivative of the contact variational form can be obtained by combining Eqs. (72) and (74) as

$$b_\Gamma^*({}^{n+1}z; \Delta\dot{z}, \bar{z}) = b_N^*({}^{n+1}z; \Delta\dot{z}, \bar{z}) + b_T^*({}^{n+1}z; \Delta\dot{z}, \bar{z}) \tag{77}$$

$$b_V'({}^{n+1}z, \bar{z}) = b_N^*({}^{n+1}z, \bar{z}) + b_T'({}^{n+1}z, \bar{z}) \tag{78}$$

C. Shape DSA Equation and Updating Sensitivity Formula

By combining the material derivative formulas in Eq. (64) for the structural energy form and Eqs. (72) and (74) for the contact variational form, the design sensitivity equation for perturbed design in Eq. (48) becomes

$$a_\Omega^*({}^{n+1}z; \Delta\dot{z}, \bar{z}) + b_\Gamma^*({}^{n+1}z; \Delta\dot{z}, \bar{z}) = \mathscr{L}_V(\bar{z}) - a_V'({}^{n+1}z, \bar{z}) - b_V'({}^{n+1}z, \bar{z}), \qquad \forall \bar{z} \in Z \tag{79}$$

Note that the solution of Eq. (79) solves for the incremental displacement sensitivity $\Delta\dot{z}$. The total displacement sensitivity is then computed by

$${}^{n+1}\dot{z} = {}^{n}\dot{z} + \Delta\dot{z} \tag{80}$$

After computing the incremental displacement sensitivity by solving Eq. (79), the Cauchy stress and internal variables are updated. The updating formula for the Cauchy stress is the same as Eq. (62) and the updating formula for the internal evolution variables are given by

$$\frac{\mathrm{d}}{\mathrm{d}\tau}({}^{n+1}\boldsymbol{\alpha}) = \frac{\mathrm{d}}{\mathrm{d}\tau}({}^{n}\boldsymbol{\alpha}) + \boldsymbol{N}\left(H_\alpha + \sqrt{\frac{2}{3}}H_\alpha'\hat{\gamma}\right)\frac{\mathrm{d}}{\mathrm{d}\tau}(\hat{\gamma}) + H_\alpha\hat{\gamma}\frac{\mathrm{d}}{\mathrm{d}\tau}(\boldsymbol{N}) \tag{81}$$

$$\frac{\mathrm{d}}{\mathrm{d}\tau}\left({}^{n+1}\hat{e}_p\right) = \frac{\mathrm{d}}{\mathrm{d}\tau}\left({}^{n}\hat{e}_p\right) + \sqrt{\frac{2}{3}}\frac{\mathrm{d}}{\mathrm{d}\tau}(\hat{\gamma}) \tag{82}$$

Note that the cost of the sensitivity computation for the elasto–plastic material is relatively expensive compared to the elastic material because of the need to update the material derivatives of the stress and internal variables at each integration point.

IV. Reproducing Kernel Particle Method (RKPM)

The continuum-based variational Eqs. (45) and (79) are discretized in the domain. Liu et al.[21] developed the reproducing kernal particle method (RKPM) by introducing a modified kernel function that is constructed based on the enforcement of reproducing conditions such that the kernel estimate of the displacement exactly

reproduces polynomials. In RKPM, a displacement function $z(x)$ is approximated using a kernel estimate as

$$z^R(x) = \int_\Omega C(x; y-x)\phi_a(y-x)z(y)\,\mathrm{d}y \tag{83}$$

where $z^R(x)$ is the reproduced displacement function of $z(x)$, $\phi_a(y-x)$ is the kernel function (or weight function) with a support measure of a, and $C(x; y-x)$ is the correction function defined by

$$C(x; y-x) = \boldsymbol{q}(x)^T \boldsymbol{H}(y-x) \tag{84}$$

where $\boldsymbol{H}(x)^T = [1, x, x^2, \ldots, x^n]$ and $\boldsymbol{q}(x)^T = [q_0(x), q_1(x), \ldots, q_n(x)]$ are the interpolation function and unknown coefficient vector, respectively. In Eq. (84), $\boldsymbol{q}(x)$ is determined by imposing the nth-order completeness requirement, where $z^R(x)$ in Eq. (83) can represent $z(x)$ completely up to the nth-order derivatives. After imposing the completeness condition,

$$z^R(x) = \int_\Omega C(x; y-x)\phi_a(y-x)z(y)\,\mathrm{d}y$$

$$= \boldsymbol{H}(0)^T \boldsymbol{M}(x)^{-1} \int_\Omega \boldsymbol{H}(y-x)\phi_a(y-x)z(y)\,\mathrm{d}y \tag{85}$$

where

$$\boldsymbol{M}(x) = \begin{bmatrix} m_0(x) & m_1(x) & \cdots & m_n(x) \\ m_1(x) & m_2(x) & \cdots & m_{n+1}(x) \\ \cdot & \cdot & \cdots & \cdot \\ m_n(x) & m_{n+1}(x) & \cdots & m_{2n}(x) \end{bmatrix} \tag{86}$$

$$\boldsymbol{H}(0)^T = [1, 0, \ldots, 0] \tag{87}$$

$$m_n(x) = \int_\Omega (y-x)^n \phi_a(y-x)\,\mathrm{d}y$$

To develop a shape function for discrete approximation, Eq. (85) must be discretized. Suppose that the domain Ω is discretized by a set of nodes $[x_1, \ldots, x_{NP}]$, where x_I is the location of node I, and NP is the total number of nodes. Using a simple trapezoidal rule, Eq. (85) is discretized into

$$z^R(x) = \sum_{I=1}^{\mathrm{NP}} C(x; x_I - x)\phi_a(x_I - x)z_I \Delta x_I \tag{88}$$

where Δx_I is a measure of length associated with node I. It is hard to determine Δx_I in a multidimensional case but it can be treated as a weight of the nodal value. However, its effect will be canceled if we compute moment $\boldsymbol{M}(x)$ in Eq. (86) consistently with Eq. (88) because its inverse is multiplied. Equation (88) can be rewritten, using the generalized displacement d_I, as

$$z^R(x) = \sum_{I=1}^{\mathrm{NP}} \Phi_I(x)\, d_I \tag{89}$$

where $\Phi_I(x) = C(x; x_I - x)\phi_a(x_I - x)$. The function $\Phi_I(x)$ is interpreted as the particle or mesh-free shape function at node I, and d_I is the associated coefficient of approximation, often called the generalized displacement. The shape function $\Phi_I(x_J)$ depends on the current coordinate x_J, whereas the shape function of the finite element method depends only on a coordinate of the reference geometry. Note that, in general, the shape function does not have the Kronecker delta properties, that is, $\Phi_I(x_J) \neq \delta_{IJ}$. Therefore, for a general function $z(x)$ that is not a polynomial, d_I in Eq. (89) is not the nodal value of $z(x)$. For the essential boundary conditions (i.e., the prescribed value at node points), the Lagrange multiplier method may be used to impose those conditions.[23] If the problem contains many boundary conditions, then the excessive number of the Lagrange multiplier greatly increases the size of the system matrix. The positive semidefiniteness of the system matrix also needs a special treatment in the solution phase. For the case of the contact problem, because contact constraints are imposed through the physical coordinate of the material point, it is inconvenient or impossible to use the generalized displacement. Chen et al.[24] proposed a direct transformation method to treat these problems systematically.

For numerical examples in this paper, a combined linear isotropic/kinematic hardening model is used with $\kappa(\hat{e}_p) = Y_0 + (1-\beta)H\hat{e}_p$ and $H_\alpha = \frac{2}{3}\beta H$. The yield function and hardening law can be defined as

$$f(\boldsymbol{\eta}, \hat{e}_p) \equiv \|\boldsymbol{\eta}\| - \sqrt{\tfrac{2}{3}}[Y_0 + (1-\beta)H\hat{e}_p] = 0 \tag{90}$$

$$\dot{\boldsymbol{\alpha}} = \tfrac{2}{3}\beta H \gamma \boldsymbol{N} \tag{91}$$

where H is the plastic modulus, which is constant for this model. Here, $\beta \in [0, 1]$ is a parameter to consider the Baushinger effect; β is equal to 1 for the kinematic hardening and is equal to zero for the isotropic hardening.

V. Numerical Examples

A. Shape DSA and Optimization of Metal Ring Contact Problem

A metal ring is used frequently as a structural component to make the seal between parts airtight with enough compressive force. The ring is generally installed tightly and local material yielding occurs as a result of excessive external compressive force. Large plastic strain causes material fracture and eventually reduces the performance of the ring by lowering the pressure on contact surfaces.

The metal ring shown in Fig. 4 is compressed by an upper rigid wall and is in contact with a fixed lower rigid wall. The inner/outer radii of the ring are 3 and 5 cm, respectively. The domain is discretized by 144 particles for the ring, 4 master nodes for the rigid wall, and 22 contact pairs (slave nodes/master segments) with frictional contact conditions. Analysis data include the contact penalty parameter 10^5, Young's modulus 206.9 GPa, Poisson's ratio 0.29, initial yield stress 1.0 GPa, hardening modulus 1.0 GPa, and $\beta = 0.5$, which is the parameter used to represent a combined isotropic/kinematic hardening model. For analysis, an RKPM (mesh-free method) with a finite supporting region size of 1×1 cm per node is used.

Nonlinear response analysis is carried out with 20 load steps by a displacement driven procedure using the Newton method. Figure 5 is a deformed configuration with a contour plot for the effective plastic strain. Five nodes are in contact with upper and lower rigid wall, respectively. Excessive plastic strain is observed at the horizontal region of the inner surface. Considering that 0.5 is usually used as a criterion of material fracture for the effective plastic strain, the maximum value of 0.294 must be reduced through design change. The inner/outer radii of the metal ring are selected as design parameters as shown in Fig. 4. The circular boundary of the ring is approximated by four segments of cubic spline curve. The control points of these curves are used as shape design parameters. Even though the original spline curves approximate a circle well enough, the circular shape may not be preserved as the shape design changes. The effect of radius change is obtained by linking four control points of curves along the circumference. The boundary design velocity field is obtained by selecting a boundary curve corresponding to the

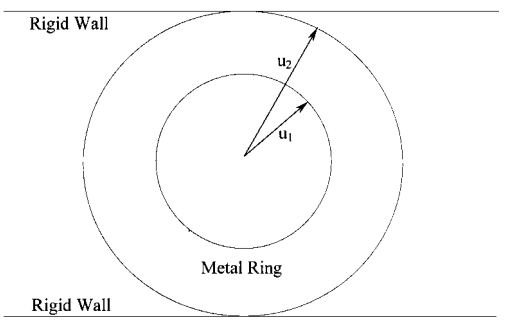

Fig. 4 Geometry and design parameters of ring contact problem.

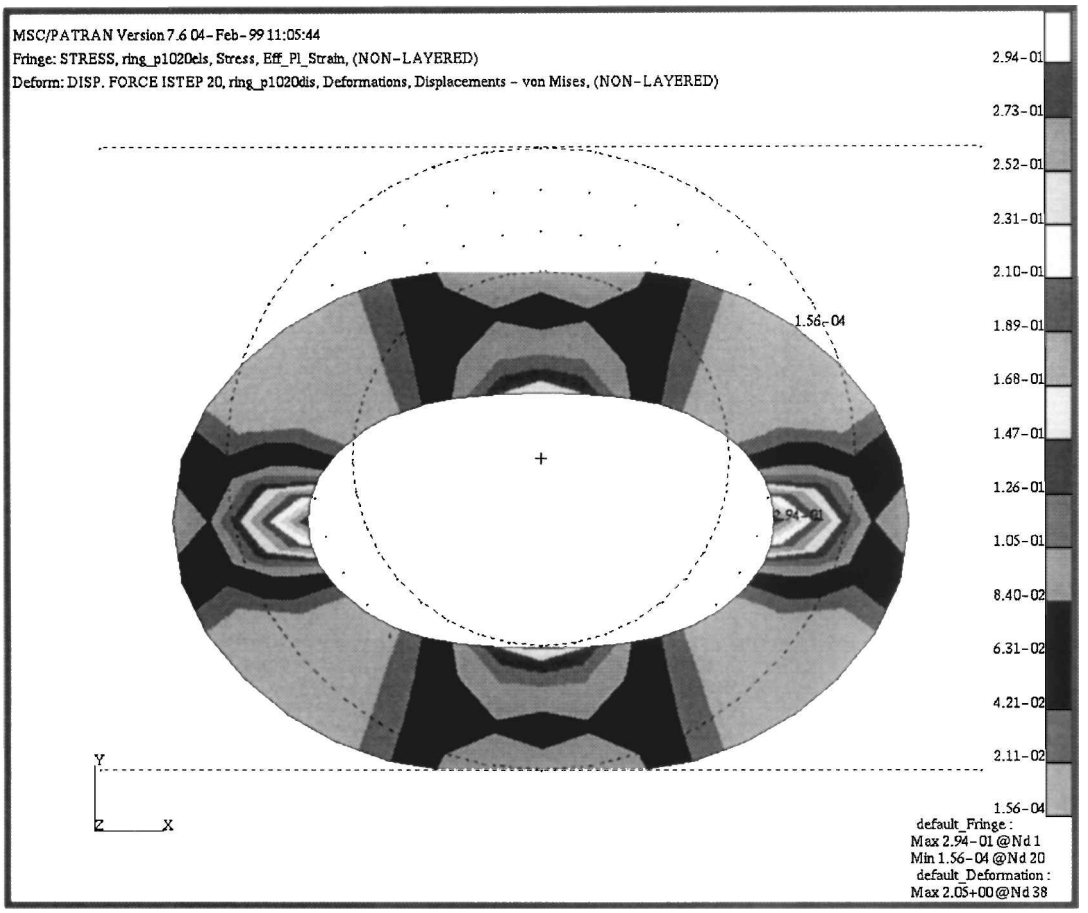

Fig. 5 Contour plot of the effective plastic strain with deformation.

design parameters, and the domain design velocity fields are computed using the isoparametric mapping method.[25] Design sensitivity analysis is carried out at each converged load step. As discussed in Sec. III, the DSA procedure for the elasto–plastic material is classified into two parts. The first is computing the material derivative of the displacement by solving the linear system of Eq. (79), and the second is updating the path-dependent variables using the displacement sensitivity computed earlier. The results of response analysis, design velocity information, and the material derivative of the stress and internal plastic variables at the earlier load step are used to compute the material derivative of the incremental displacement at the current load step. The material derivative of the stress and internal plastic variables are stored in the global array for each integration point.

Table 1 lists shape design sensitivities of various performance measures with respect to changes of the inner and outer radii, respectively. The results obtained using the proposed method agree very well with those obtained by the forward finite difference method. The total response analysis CPU time is 242 s, and the sensitivity computation CPU time is 12 s. for two design parameters using an Hewlett–Packard Company workstation. Thus, sensitivity computation per design variable is only 2.5% of the analysis time. In Table 1, the third column $\Delta\Psi$ denotes the first-order sensitivity results from forward finite difference method with a perturbation of $\tau = 10^{-6}$, and the fourth column represents sensitivity computation result of the proposed method. In the first column, $\hat{e}^p$, σ, and F_C denote effective plastic strain, von Mises stress invariant, and the normal contact force, respectively. For example, $\hat{e}^p_{28}$ denotes the effective plastic strain at integration zone 28, and F_{Cy} denotes the sum of all of the contact forces along the lower rigid wall.

As mentioned, the excessive effective plastic strain has to be reduced while the normal contact force through the rigid wall is maintained. The area of the metal ring is to be minimized with constraints on the effective plastic strain at integration zone 3 and the sum of the normal contact forces. Two design parameters range in the interval $[-1, 1]$ with zero initial values. The design optimization problem can be formulated as

$$\begin{array}{lll} \text{MIN} & \text{area} & \\ \text{subject to} & \hat{e}^p(0.3) \le 0.1 & F_{Cy}(2.18) \ge 2.18 \\ & -1.0 \le u_1 \le 1.0 & -1.0 \le u_2 \le 1.0 \end{array} \tag{92}$$

where the values in the parenthesis are the performance values of the original design.

Design optimization is carried out using the sequential quadratic programming (SQP) method in DOT.[26] The performance values are supplied to DOT from nonlinear response analysis (RKPM), and the sensitivity coefficients are provided by the proposed method. The initial design is infeasible because one constraint is violated. Optimization is converged after five iterations and all of the constraints are satisfied. The cost function, which is the area of the ring, is reduced by up to 10% of the original design, and the normal contact force is maintained as the original one. The effective plastic strain, however, is decreased significantly, by up to 95% of the original design. Figure 6 shows the optimized design and the results of response analysis. The original circular surface is changed to a different shape at the optimum design. The optimization algorithm chooses a new design such that the effective plastic strain is distributed evenly between inner surfaces, whereas the original design has a concentration at the horizontal regions.

Figure 7 shows the design history of the cost function, constraints, and design parameters. The design parameters are converged to values within the bounds, and the contact force constraint remains active.

B. Design Sensitivity Analysis of Metal Punch Problem

The punch problem is commonly used in the manufacturing process to make parts of a certain shape. Because the process is based

Table 1 Sensitivity analysis results and comparison with finite difference method

Performance	Ψ	$\Delta\Psi$	Ψ'	$(\Delta\Psi/\Psi')\times 100\%$
		u_1		
Area	$0.498139E+02$	$-0.158418E-04$	$-0.158418E-04$	100.00
$\hat{e}^p_{28}$	$0.166961E+00$	$0.300634E-06$	$0.300633E-06$	100.00
$\hat{e}^p_{79}$	$0.166954E+00$	$0.300641E-06$	$0.300641E-06$	100.00
$\hat{e}^p_{82}$	$0.166961E+00$	$0.300630E-06$	$0.300630E-06$	100.00
$\hat{e}^p_{1}$	$0.293886E+00$	$0.209079E-07$	$0.209080E-07$	100.00
$\hat{e}^p_{52}$	$0.293880E+00$	$0.209178E-07$	$0.209179E-07$	100.00
$\hat{e}^p_{55}$	$0.293887E+00$	$0.209051E-07$	$0.209052E-07$	100.00
$\hat{e}^p_{106}$	$0.293880E+00$	$0.209172E-07$	$0.209174E-07$	100.00
σ_1	$0.129381E+01$	$0.210710E-07$	$0.210711E-07$	100.00
σ_{52}	$0.129380E+01$	$0.210808E-07$	$0.210810E-07$	100.00
σ_{55}	$0.129381E+01$	$0.210682E-07$	$0.210683E-07$	100.00
σ_{106}	$0.129380E+01$	$0.210803E-07$	$0.210804E-07$	100.00
F_{Cy}	$0.218260E+01$	$-0.253422E-05$	$-0.253423E-05$	100.00
		u_2		
Area	$0.498139E+02$	$0.264031E-04$	$0.264031E-04$	100.00
$\hat{e}^p_{28}$	$0.166961E+00$	$-0.271065E-06$	$-0.271065E-06$	100.00
$\hat{e}^p_{79}$	$0.166954E+00$	$-0.271094E-06$	$-0.271094E-06$	100.00
$\hat{e}^p_{82}$	$0.166961E+00$	$-0.271062E-06$	$-0.271063E-06$	100.00
$\hat{e}^p_{1}$	$0.293886E+00$	$0.184466E-06$	$0.184466E-06$	100.00
$\hat{e}^p_{52}$	$0.293880E+00$	$0.184439E-06$	$0.184440E-06$	100.00
$\hat{e}^p_{55}$	$0.293887E+00$	$0.184467E-06$	$0.184467E-06$	100.00
$\hat{e}^p_{106}$	$0.293880E+00$	$0.184439E-06$	$0.184440E-06$	100.00
σ_1	$0.129381E+01$	$0.184079E-06$	$0.184079E-06$	100.00
σ_{52}	$0.129380E+01$	$0.184053E-06$	$0.184053E-06$	100.00
σ_{55}	$0.129381E+01$	$0.184080E-06$	$0.184081E-06$	100.00
σ_{106}	$0.129380E+01$	$0.184053E-06$	$0.184053E-06$	100.00
F_{Cy}	$0.218260E+01$	$0.260354E-05$	$0.260350E-05$	100.00

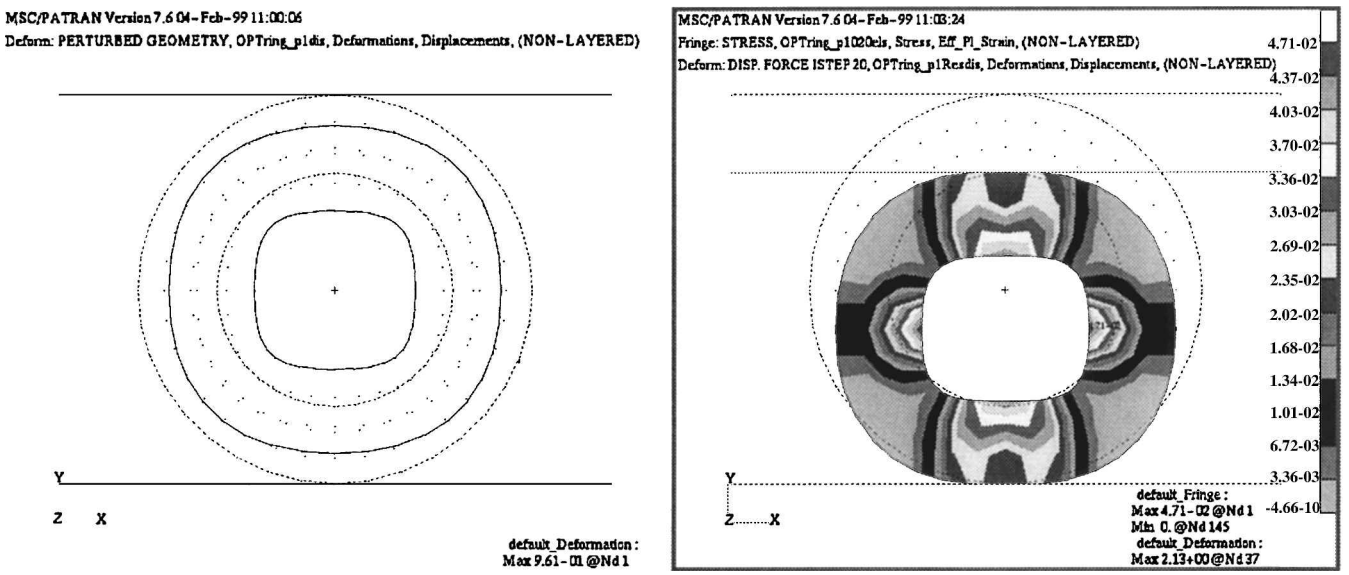

Fig. 6 Optimized design and response analysis results.

on the plastic deformation of metal parts, controlling plastic deformation and elastic springback is important to the quality of the product. Excessive amount of plastic strain frequently causes local fracture of the material during the manufacturing process. However, elastic springback makes it difficult to determine the final shape of the product after removing the punch. This example shows a simple punch problem where the thickness of metal plate and the radius of circular punch can be changed with different constitutive models.

Figure 8 shows the initial geometry of a metal plate punch problem with a cylindrical rigid punch. The radius of the rigid punch is 8.0 cm. The lower right rigid wall is fixed, and the upper left punch moves downward 1.0 cm. A small deformation is chosen to consider the small deformation elasto–plastic constitutive model. The domain is discretized using 93 RKPM particles and 40 piecewise linear master segments to define the geometry of the rigid wall. An infinitesimal elasto–plastic material is used with Young's modulus $E = 206.9$ GPa, Poisson's ratio $\nu = 0.29$, plastic hardening modulus $H = 1.1$ GPa, and initial yield stress $\sigma_y = 0.5$ GPa. The linear isotropic hardening is considered where the plastic consistency condition can be solved explicitly without iteration. Frictional contact constraints are imposed between the sheet metal and rigid wall with a friction coefficient of $\mu = 0.2$. The symmetric boundary conditions are imposed on each end of the sheet metal.

Nonlinear response analysis is carried out with 100 load steps using the standard Newton–Raphson method. After the solution is converged for the given load step, the decomposed tangent stiffness matrix is stored for DSA. Figure 9 shows the deformed shape with a contour plot for the effective plastic strain. Because the deformation

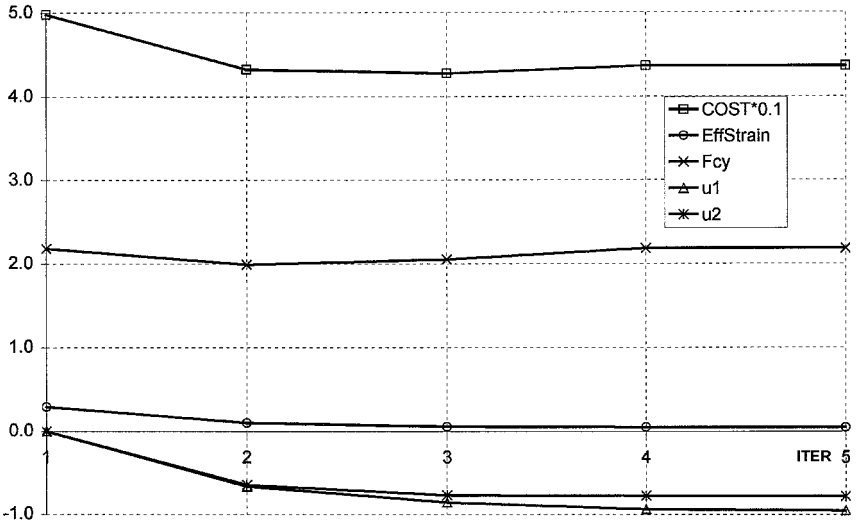

Fig. 7 Design optimization history of metal ring contact problem.

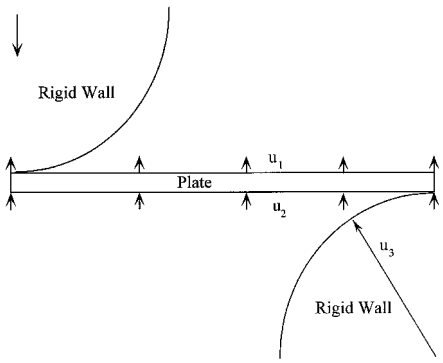

Fig. 8 Geometry and design parameters of plate punch problem.

is small, most parts of material maintain an elastic status, whereas plastic deformation is concentrated at both ends.

The DSA starts by choosing design parameters and computing design velocity fields for the shape design parameters. The first design parameter moves the upper boundary of the plate and the second one moves the lower boundary. Because the two design parameters have opposite effects on the structure, we can expect that the sensitivity coefficients of two design parameters will have the same magnitude but with opposite signs. The third design parameter is the radius of the right lower rigid wall. A nonlinear DSA is carried out at each converged load step to compute the material derivative of displacement with the same tangent stiffness matrix as response analysis without iteration. After computing the displacement sensitivity, the material derivative of the Cauchy stress and internal plastic variables are updated using the formulas given in Eqs. (62), (81), and (82). Table 2 shows the sensitivity coefficients where the sensitivity results are very well matched with the finite difference results. The nonlinear response analysis converged to the final load step in 196 s of CPU time, whereas DSA for three design parameters requires 52 s. This means that the cost of sensitivity computation is only 9% of the response analysis time per each design parameter, which is quite efficient compared to the finite difference method.

VI. Difficulties in DSA for a Finite Deformation Problem

For the geometric nonlinear problem, it is convenient to choose the current configuration as the reference frame because of the evolution equation in the plasticity. The constitutive relation and the return mapping algorithm are given with respect to the current configuration. However, from the DSA point of view, because the design is perturbed at the undeformed structure, the material derivative must be taken at the undeformed configuration for a given design velocity field. It is necessary to transform the spatial strain tensor to the undeformed configuration using the deformation gradient. If the classical plasticity theory is used for analysis, the material derivative of the incremental strain must be taken during the DSA procedure as

$$\frac{\mathrm{d}}{\mathrm{d}\tau}(\Delta\varepsilon) = \frac{\mathrm{d}}{\mathrm{d}\tau}\frac{1}{2}\left[\nabla_0(\Delta z)\boldsymbol{F}^{-1} + \boldsymbol{F}^{-T}\nabla_0(\Delta z)^T\right] \tag{93}$$

where $\nabla_0 = \partial/\partial^0\boldsymbol{x}$ is the derivative with respect to the initial coordinate. Because the inverse of the deformation gradient exists in Eq. (93), additional terms that contain the total displacement sensitivity exist and yield a stiffness matrix different from that of analysis.

As shown in earlier sections, if the infinitesimal deformation is assumed, then the preceding discussion does not have to be considered because the reference configuration is always undeformed, and there is no need to update the configuration. Thus, most of the research results in the Refs. 3, 5, 7, 9, and 10 succeed based on the infinitesimal deformation assumption. Kleiber[8] tried to resolve this problem by establishing a reference configuration using the previously converged time without numerical examples. However, the constitutive relation must be expressed in terms of second Piola–Kirchhoff stress, which is inconvenient for the plasticity model. Because all configurations at the previous time are known, sensitivity formulation is similar to that of the total Lagrangian formulation. Zhang et al.[6] proposed a large deformation sensitivity problem using the boundary-element method. They computed the displacement sensitivity by iteration, which may significantly increase the cost of the sensitivity computation. Dutta[27] discussed a similar approach where the sensitivity equation has a different stiffness matrix from the analysis stiffness matrix. He proposed an iterative method to compute the sensitivity using the same stiffness matrix as the one used for analysis. All of these difficulties stem from the existence of a deformation gradient or its inverse in the strain measure. However, in the theoretical sense, if the stiffness matrix of analysis is the exact tangent operator, then the sensitivity equation must use the same tangent operator. Sensitivity or response analyses will yield erroneous results or slow convergence if we use other than the exact tangent operator.

Consider the following incremental elastic constitutive relation:

$$^{n+1}\boldsymbol{S} = {}^{n}\boldsymbol{S} + \boldsymbol{C} : \Delta\boldsymbol{E} \tag{94}$$

where C_{ijkl} could be constant or a function of deformation. Is the sensitivity of this material model path dependent? Obviously, analysis itself is path independent, which means that the same result will be obtained even if a different path is chosen. However, if we take the material derivative of Eq. (94), then the sensitivity equation becomes path dependent because it needs the sensitivity information from the preceding time or, at least, one cannot solve the sensitivity

Table 2 Sensitivity analysis results and comparison with finite difference method

Performance	Ψ	$\Delta\Psi$	Ψ'	$(\Delta\Psi/\Psi')\times 100\%$
		u_1		
z_{y20}	$-0.149013\,E+00$	$-0.201625\,E-06$	$-0.201625\,E-06$	100.00
z_{y40}	$-0.420559\,E+00$	$-0.438457\,E-06$	$-0.438457\,E-06$	100.00
$\hat{e}^p_{59}$	$0.569335\,E-02$	$0.226768\,E-07$	$0.226768\,E-07$	100.00
$\hat{e}^p_{57}$	$0.276513\,E-02$	$0.151480\,E-07$	$0.151480\,E-07$	100.00
F_{Cy1}	$0.154504\,E-01$	$0.347529\,E-07$	$0.347527\,E-07$	100.00
F_{Cy93}	$-0.154504\,E-01$	$-0.347528\,E-07$	$-0.347527\,E-07$	100.00
g_{n4}	$0.665325\,E-02$	$-0.165339\,E-07$	$-0.165339\,E-07$	100.00
g_{n90}	$0.187188\,E-01$	$-0.165320\,E-07$	$-0.165320\,E-07$	100.00
		u_2		
z_{y20}	$-0.149013\,E+00$	$0.201625\,E-06$	$0.201625\,E-06$	100.00
z_{y40}	$-0.420559\,E+00$	$0.438457\,E-06$	$0.438457\,E-06$	100.00
$\hat{e}^p_{59}$	$0.569335\,E-02$	$-0.226767\,E-07$	$-0.226768\,E-07$	100.00
$\hat{e}^p_{57}$	$0.276513\,E-02$	$-0.151480\,E-07$	$-0.151480\,E-07$	100.00
F_{Cy1}	$0.154504\,E-01$	$-0.347526\,E-07$	$-0.347527\,E-07$	100.00
F_{Cy93}	$-0.154504\,E-01$	$0.347529\,E-07$	$0.347527\,E-07$	100.00
g_{n4}	$0.665325\,E-02$	$0.165339\,E-07$	$0.165339\,E-07$	100.00
g_{n90}	$0.187188\,E-01$	$0.165320\,E-07$	$0.165320\,E-07$	100.00
		u_3		
$z_{y\,20}$	$-0.149013\,E+00$	$-0.826317\,E-06$	$-0.826317\,E-06$	100.00
$z_{y\,40}$	$-0.420559\,E+00$	$-0.572741\,E-06$	$-0.572741\,E-06$	100.00
$\hat{e}^p_{59}$	$0.569335\,E-02$	$-0.128969\,E-07$	$-0.128969\,E-07$	100.00
$\hat{e}^p_{57}$	$0.276513\,E-02$	$-0.672229\,E-08$	$-0.672229\,E-08$	100.00
F_{Cy1}	$0.154504\,E-01$	$-0.169642\,E-08$	$-0.169648\,E-08$	100.00
$F_{Cy\,93}$	$-0.154504\,E-01$	$0.169659\,E-08$	$0.169648\,E-08$	100.01
$g_{n\,4}$	$0.665325\,E-02$	$0.197133\,E-07$	$0.197133\,E-07$	100.00
$g_{n\,90}$	$0.187188\,E-01$	$0.121685\,E-07$	$0.121685\,E-07$	100.00

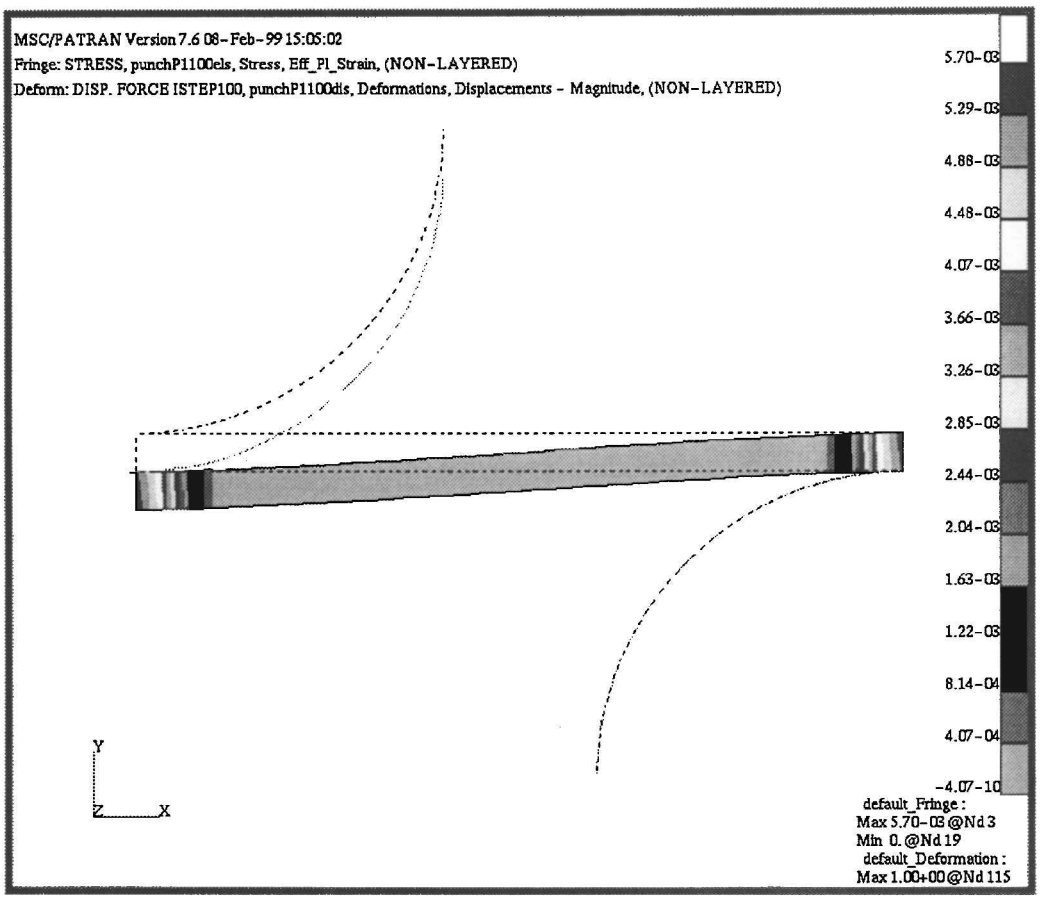

Fig. 9 Contour plot of the effective plastic strain with deformation.

equation at the final converged time only. Note that the tangent operator for sensitivity analysis corresponding to Eq. (94) is different from the stiffness matrix for analysis.

VII. Conclusions

A continuum-based design sensitivity formulation for the elasto–plasticity material with a frictional contact problem is proposed. The path dependency of the sensitivity equation comes from the constitutive relation and frictional phenomenon. Numerical examples show the accurate results of the proposed method with quite efficient computational time.

Acknowledgments

This research is partially supported by the Automotive Research Center sponsored by the U.S. Army Tank Automotive Research Development and Engineering Center and the National Science Foundation/Defense Advanced Research Projects Agency, Optimized Portable Algorithms and Applications Libraries, under Contract 9874015.

References

[1]Haug, E. J., Choi, K. K., and Komkov, V., *Design Sensitivity Analysis of Structural Systems*, Academic, New York, 1986.

[2]Duvaut, G., and Lions, J. L., *Inequalities in Mechanics and Physics*, Spring-Verlag, Berlin, 1976.

[3]Vidal, C. A., and Haber, R. B., "Design Sensitivity Analysis for Rate-Independent Elastoplasticity," *Computer Methods in Applied Mechanics and Engineering*, Vol. 107, No. 3, 1993, pp. 393–431.

[4]Simo, J. C., and Taylor, R. L., "Consistent Tangent Operator for Rate-Independent Elastoplasticity," *Computer Methods in Applied Mechanics and Engineering*, Vol. 48, No. 1, 1985, pp. 101–118.

[5]Lee, T. H., and Arora, J. S., "A Computational Method for Design Sensitivity Analysis of Elastoplastic Structures," *Computer Methods in Applied Mechanics and Engineering*, Vol. 122, No. 1, 1995, pp. 27–50.

[6]Zhang, Q., Mukherjee, S., and Chandra, A., "Shape Design Sensitivity Analysis for Geometrically and Materially Nonlinear Problems by the Boundary Element Method," *International Journal of Solids and Structures*, Vol. 29, 1992, pp. 2503–2525.

[7]Park, Y. H., and Choi, K. K., "Design Sensitivity Analysis of Truss Structures with Elastoplastic Material," *Mechanics of Structures and Machines*, Vol. 24, No. 2, 1996, pp. 189–216.

[8]Kleiber, M., "Shape and Non-Shape Structural Sensitivity Analysis for Problems with any Material and Kinematic Non-Linearity," *Computer Methods in Applied Mechanics and Engineering*, Vol. 108, No. 1, 1993, pp. 73–97.

[9]Michaleris, P., Tortorelli, D. A., and Vidal, C. A., "Tangent Operators and Design Sensitivity Formulations for Transient Non-Linear Coupled Problems with Applications to Elastoplasticity," *International Journal for Numerical Methods in Engineering*, Vol. 37, No. 14, 1994, pp. 2471–2499.

[10]Ohsaki, M., and Arora, J. S., "Design Sensitivity Analysis of Elastoplastic Structures," *International Journal for Numerical Methods in Engineering*, Vol. 37, No. 5, 1994, pp. 737–762.

[11]Kikuchi, N., and Oden, J. T., "*Contact Problems in Elasticity: a Study of Variational Inequalities and Finite Element Method*, Society for Industrial and Applied Mathematics, Philadelphia, 1988.

[12]Hughes, T. J. R., Taylor, R. L., Sackman, J. L., Curnier, A., and Kanoknukulchai, W., "A Finite Element Method for a Class of Contact-Impact Problems," *Computer Methods in Applied Mechanics and Engineering*, Vol. 8, 1976, pp. 249–276.

[13]Simo, J. C., Wriggers, P., and Taylor, R. L., "A Perturbed Lagrangian Formulation for the Finite Element Solution of Contact Problems," *Computer Methods in Applied Mechanics and Engineering*, Vol. 50, No. 2, 1985, pp. 163–180.

[14]Simo, J. C., and Laursen, T. A., "An Augmented Lagrangian Treatment of Contact Problems Involving Friction," *Computers and Structures*, Vol. 42, No. 1, 1992, pp. 97–116.

[15]Mignot, F., "Controle Dans Les Inequations Variationelles Elliptiques," *Journal of Functional Analysis*, Vol. 22, 1976, pp. 130–185.

[16]Haraux, A., "How to Differentiate the Projection on a Convex Set in Hilbert Space. Some Applications to Variational Inequalities," *Journal of Mathematical Society of Japan*, Vol. 29, 1977, pp. 615–631.

[17]Sokolowski, J., and Zolesio, J. P., *Introduction to Shape Optimization*, Springer-Verlag, Berlin, 1991.

[18]Spivey, C. O., and Tortorelli, D. A., "Tangent Operators, Sensitivity Expressions, and Optimal Design of Nonlinear Elastica in Contact with Applications to Beams," *International Journal for Numerical Methods in Engineering*, Vol. 37, No. 1, 1994, pp. 49–73.

[19]Pollock, G. D., and Noor, A. K., "Sensitivity Analysis of the Contact/Impact Response of Composite Structures," *Computers and Structures*, Vol. 61, No. 2, 1996, pp. 251–269.

[20]Choi, K. K., Kim, N. H., and Park, Y. H., "Shape Design Sensitivity Analysis for Contact Problem with Friction," *Proceedings of the 7th AIAA/USAF/NASA/ISSMO Symposium on Multidisciplinary Analysis and Optimization*, AIAA, Reston, VA, 1998, pp. 1071–1081.

[21]Liu, W. K., Jun, S., and Zhang, Y. F., "Reproducing Kernel Particle Methods," *International Journal for Numerical Methods in Fluids*, Vol. 20, 1995, pp. 1081–1106.

[22]Simo, J. C., and Govindjee, S., "Nonlinear B-Stability and Symmetric Preserving Return Mapping Algorithms for Plasticity and Viscoplasticity," *International Journal for Numerical Methods in Engineering*, Vol. 31, No. 1, 1991, pp. 151–176.

[23]Grindeanu, I., Chang, K. H., Choi, K. K., and Chen, J. S., "Design Sensitivity Analysis of Hyperelastic Structures Using a Meshless Method," *AIAA Journal*, Vol. 36, No. 4, 1998, pp. 618–627.

[24]Chen, J. S., Pan, C., and Wu, C. T., "Large Deformation Analysis of Rubber Based on a Reproducing Kernel Particle Method," *Computational Mechanics*, Vol. 19, No. 3, 1997, pp. 211–217.

[25]Choi, K. K., and Chang, K. H., "A Study on the Velocity Computation for Shape Design Optimization," *Journal of Finite Elements in Analysis and Design*, Vol. 15, 1994, pp. 317–347.

[26]Vanderplaats, G. M., *DOT User's Manual*, VMA Corp., Colorado Springs, CO, 1997.

[27]Dutta, A., "A Study of Implicit and Explicit Methods for Design Sensitivity Analysis of Nonlinear Dynamic Systems," Ph.D. Dissertation, Dept. of Civil and Environment Engineering, Univ. of Iowa, Iowa City, IA, 1996.

S. Saigal
Associate Editor